Research Square

Preprints are preliminary reports that have not undergone peer review.
They should not be considered conclusive, used to inform clinical practice,
or referenced by the media as validated information.

Exercise-induced enrichment of Parabacteroides distasonis protects against osteoarthritis through an isoLCA–PGC-1α axis

Wenkang Liu
Binhai County People's Hospital
Shihan Wang
No.2 Jinkai Avenue, Liangjiang New Area, Yubei DistrictN
Mengbo Dang
The Second Affiliated Hospital of Xuzhou Medical University
Maoyuan Bian
Binhai County People's Hospital
Ying Chen
Binhai County People's Hospital
Yun Zhang
Binhai County People's Hospital
Qinfeng Huang
Binhai County People's Hospital
Pei Zhang
Department of orthopedics , Affiliated Hospital of Yangzhou University
Jin Liu
saulj163@163.com

Binhai County People's Hospital

Research Article

Keywords: Osteoarthritis, Exercise, Parabacteroides distasonis, isoLCA, PGC-1α, Chondrocyte senescence

Posted Date: November 17th, 2026

DOI: https://doi.org/10.21203/rs.3.rs-11468828/v1

License: This work is licensed under a Creative Commons Attribution 4.0 International License.
Read Full License

Additional Declarations: No competing interests reported.

Exercise-induced enrichment of Parabacteroides distasonis protects against osteoarthritis through an isoLCA–PGC-1α axis

Wenkang Liu[1,#], Shihan Wang[2,#], Mengbo Dang[3], Maoyuan Bian[1], Ying Chen[1], Yun Zhang[1], Qinfeng Huang[1], Pei Zhang[4*], Jin Liu[1*]

1 Department of Orthopedics, Binhai County People's Hospital, Yancheng, China

2 No. 2 Jinkai Avenue, Liangjiang New Area, Yubei District, Chongqing, China

3 The Second Affiliated Hospital of Xuzhou Medical University, Xuzhou, China

4 Department of orthopedics , Affiliated Hospital of Yangzhou University, Yangzhou, China

[#] These authors contributed equally

[*]Corresponding author:

Pei Zhang, zpbs28@163.com, Department of orthopedics , Affiliated Hospital of Yangzhou University, Yangzhou, China.

Jin Liu , saulj163@163.com, Department of Orthopedics, Binhai County People's Hospital, Yancheng, 224500, China.

Abstract

Background: Exercise is widely recommended for osteoarthritis (OA), but the mechanisms by which it protects articular cartilage remain incompletely understood. This study investigated whether exercise-induced alterations in the gut microbiota contribute to OA protection through microbial bile acid metabolism and chondrocyte mitochondrial regulation.

Methods: A mouse model of OA was established by destabilization of the medial meniscus (DMM). The protective effects of treadmill exercise were evaluated using histological, micro-computed tomography, and inflammatory analyses. Fecal transfer experiments, 16S rRNA sequencing, and bacterial supplementation were performed to investigate the contribution of the gut microbiota. Metabolomic profiling, metagenomic analysis, bacterial 5β-reductase deletion, and metabolite rescue experiments were used to identify the responsible microbial metabolic pathway. RNA sequencing, mitochondrial functional assays, and cartilage-specific PGC-1α deletion were employed to determine the underlying protective mechanism.

Results: Exercise significantly attenuated cartilage degeneration, synovitis, osteophyte formation, and systemic inflammation in DMM-induced OA mice. Fecal material, bacterial fractions, and cell-free metabolite fractions from exercised mice reproduced these protective effects. Exercise markedly enriched Parabacteroides distasonis, and its administration reduced joint degeneration and chondrocyte senescence. Metabolomic analysis identified isolithocholic acid (isoLCA) as a substantially elevated bile acid metabolite that reproduced the protective effects of P. distasonis. Deletion of bacterial 5β-reductase abolished these benefits, whereas exogenous isoLCA restored protection. Mechanistically, isoLCA upregulated PGC-1α expression, enhanced mitochondrial oxidative phosphorylation and respiratory capacity, reduced reactive oxygen species, and restored mitochondrial membrane potential in chondrocytes. Cartilage-specific PGC-1α deletion abolished the protective response to isoLCA in vivo.

Conclusions: Exercise-induced enrichment of P. distasonis protects against OA through a microbial 5β-reductase–isoLCA–PGC-1α signaling axis. These findings identify a gut microbiota-derived metabolic mechanism linking exercise to chondrocyte mitochondrial homeostasis and suggest potential microbiota-targeted therapeutic strategies for OA.

Keywords: Osteoarthritis; Exercise; Parabacteroides distasonis; isoLCA; PGC-1α; Chondrocyte senescence.

1 Introduction

OA is a chronic disease of the entire joint, characterized by progressive cartilage loss, synovial inflammation, osteophyte formation, and remodeling of subchondral bone. These structural changes ultimately cause pain, loss of mobility, and disability, yet disease-modifying therapies remain limited and treatment is still dominated by symptom control and joint replacement at advanced stages [1, 2]. Exercise occupies a distinctive position in OA management because it is strongly recommended across major clinical guidelines and improves pain and physical function despite imposing repeated mechanical load on the diseased joint [1, 2]. The prevailing explanation is that exercise improves muscle strength, joint stability, weight control, and load distribution. These mechanisms are important, but they do not fully account for the broad anti-inflammatory and metabolic adaptations induced by regular physical activity, nor do they explain how a systemic intervention is communicated to articular cartilage.

An emerging possibility is that the gut microbiota functions as an intermediary between exercise and distant tissues. Exercise can remodel microbial community structure and metabolic output in both humans and experimental animals, and these changes can be reversible when training ceases [3-6]. In parallel, a growing body of work implicates the intestinal microbiota in OA pathogenesis. Germ-free mice develop less severe injury-induced OA than conventionally colonized animals, and microbiota-directed interventions can alter inflammatory and structural features of disease [7, 8]. These observations establish a gut–joint connection but leave several causal questions unresolved. It remains unclear whether intestinal material is sufficient to transmit the joint-protective phenotype associated with exercise, which exercise-responsive organisms are responsible, and which microbial products act on cartilage.

Microbial bile acid metabolism provides an attractive mechanism for such long-range communication. Intestinal bacteria chemically diversify host-derived bile acids through deconjugation, oxidation, epimerization, and reduction, generating metabolites with biological activities that differ substantially from their precursors. isoLCA is a microbiota-derived stereoisomer of lithocholic acid that has been studied primarily for its ability to modulate T cell differentiation and mucosal immune homeostasis [9-11]. The generation of isoLCA-related intermediates depends on bacterial oxidoreductases, including 5β-reductase and hydroxysteroid dehydrogenases. P. distasonis is a metabolically versatile commensal capable of remodeling bile acid pools and has been associated with beneficial effects in metabolic disease and inflammatory arthritis [12-14]. Whether exercise selectively enriches P. distasonis, whether this organism generates an OA-protective bile acid program, and whether that program can be genetically ordered have not been established.

A second unresolved question is how a circulating microbial metabolite would protect cartilage. Chondrocytes in OA undergo profound metabolic reprogramming, including impaired mitochondrial biogenesis, reduced oxidative phosphorylation, increased reactive oxygen species (ROS), and activation of p16- and p21-associated senescence programs [15-17]. These changes are not merely by-products of tissue degeneration: mitochondrial dysfunction can amplify matrix catabolism, oxidative injury, and the senescence-associated

secretory phenotype. PGC-1α, encoded by PPARGC1A, is a central transcriptional coactivator that coordinates mitochondrial biogenesis, oxidative metabolism, and stress adaptation. PGC-1α activity is diminished in OA chondrocytes, whereas restoration of this pathway improves mitochondrial function and restrains catabolic responses [18, 19]. Thus, PGC-1α provides a plausible cartilage-intrinsic node through which a microbial metabolite could influence structural disease.

Here, we tested a sequential causal model linking exercise to cartilage metabolism. We first established the joint-protective phenotype of treadmill exercise and asked whether material derived from the exercise-conditioned intestinal ecosystem could transfer this phenotype to recipient mice. Microbiome profiling and direct bacterial supplementation were then used to identify an exercise-responsive organism. Metabolomics, metagenomic enzyme mapping, bacterial gene deletion, and metabolite rescue were combined to define the microbial pathway. Finally, RNA sequencing, mitochondrial functional assays, and cartilage-specific PGC-1α deletion were used to identify and genetically validate the host effector mechanism. The resulting data reveal a stepwise exercise–P. distasonis–isoLCA–PGC-1α axis that connects physical activity to chondrocyte mitochondrial fitness and suppression of OA.

2 Methods

2.1 Mice

Male C57BL/6 mice were obtained at 6 weeks of age and maintained under specific-pathogen-free conditions with a 12-h light/dark cycle, controlled temperature and humidity, standard chow, and water ad libitum. Animals were acclimated before experimental manipulation. Ppargc1a-floxed mice were crossed with Col2a1-CreERT2 mice to generate inducible cartilage-lineage PGC-1α-deficient animals and Ppargc1a^fl/fl littermate controls. Recombination was induced with tamoxifen before DMM surgery and genotypes were confirmed by PCR. Mice were randomly allocated to treatment groups, and investigators responsible for histological scoring, micro-CT quantification, and image analysis were blinded to group identity. All animal procedures were approved by the responsible institutional animal-care and use committee (Experimental Animal Ethics Committee of Yangzhou University, NO: yzu-lcyxy-n008) and were conducted in accordance with

national guidelines for laboratory animal welfare.

2.2 Primary articular chondrocytes

Primary mouse articular chondrocytes were isolated from knee cartilage under sterile conditions. Cartilage was dissected free of bone and soft tissue, minced, and sequentially digested with 0.25% trypsin–EDTA for 30 min followed by 0.2% collagenase type II for 4–6 h at 37°C with gentle agitation. Released cells were passed through a 70-μm strainer, washed, and cultured in DMEM/F-12 supplemented with 10% fetal bovine serum and 1% penicillin–streptomycin at 37°C in 5% CO_2. Early-passage cells from independent isolations were used for experiments.

2.3 Exercise protocol in mice

Forced exercise was performed using a motorized treadmill for small animals. Mice were divided into control and exercise groups. The exercise protocol consisted of running at a speed of 10 m/min on a 5° incline, for 30 min per day, five days per week. Mice in the exercise group underwent training for a total of 8 weeks. At the end of the intervention, mice were anesthetized for DMM surgery.

2.4 Destabilization of the medial meniscus model

Experimental knee OA was induced by destabilization of the medial meniscus (DMM). Mice were anesthetized with inhaled isoflurane (3% for induction and 1.5–2% for maintenance) delivered in oxygen via a small-animal inhalation anesthesia system. Anesthetic depth was assessed by monitoring respiratory rate and the response to pedal withdrawal stimulation. Under anesthesia, the medial aspect of the knee was prepared aseptically, and the joint capsule was opened through a small medial parapatellar approach. The medial meniscotibial ligament was identified and transected without damaging the articular surface. The joint capsule and skin were closed in layers, and mice received perioperative analgesia and postoperative monitoring. Sham procedures, where used, included the same surgical exposure without transection of the medial meniscotibial ligament. Animals were followed to the prespecified experimental endpoint.

At the predetermined experimental endpoint, mice were euthanized by CO_2 inhalation. Briefly, 100% CO_2 was gradually introduced into a chamber (approximately 7 L) at a volume displacement rate of 50% per minute (approximately 3.5 L/min). After 2 min of active

exposure, the gas supply was turned off, and the chamber remained closed for an additional 3 min. Death was confirmed by the absence of spontaneous respiration and heartbeat before knee joint collection for subsequent analyses.

2.5 Fecal collection, fractionation, and transfer

Fresh fecal pellets were collected from exercised donor mice into sterile tubes and processed immediately under oxygen-limited conditions. Whole fecal material was suspended in sterile reduced PBS and clarified to remove coarse particulate matter. A microbial cellular fraction was recovered by differential centrifugation, washed, and resuspended in the original vehicle. The corresponding supernatant was passed through a sterilizing membrane to generate a cell-free metabolite fraction. All preparations were normalized to the same starting fecal mass. Recipient mice received vehicle, whole fecal suspension, microbial fraction, or sterile metabolite fraction by oral gavage every other day beginning before DMM surgery and continuing through the experimental period.

2.6 16S rRNA gene sequencing and microbiome analysis

Fecal samples from control and exercised mice were snap-frozen and stored at −80°C. Microbial DNA was extracted using a bead-beating stool DNA workflow. DNA concentration and purity were assessed fluorometrically and spectrophotometrically, and integrity was verified by agarose gel electrophoresis. The V3–V4 region of the bacterial 16S rRNA gene was amplified using primers 341F and 806R. Amplicons were purified, indexed, pooled at equimolar concentrations, and sequenced as paired-end reads on an Illumina platform. Raw reads were demultiplexed, adapter- and primer-trimmed, filtered for quality, and screened for chimeras. Amplicon sequence variants were inferred with DADA2 in QIIME 2 and taxonomically assigned against the SILVA database. Bray–Curtis dissimilarity was used for principal coordinate analysis, and group differences were assessed by PERMANOVA. Relative-abundance profiles, heatmaps, and LEfSe analysis were used to identify exercise-associated taxa. P. distasonis abundance was extracted from the feature table and used to prioritize the bacterial intervention experiment.

2.7 P. distasonis administration

Fresh P. distasonis cultures were washed and adjusted to 1 × 10^8 CFU per dose. Mice received bacterial suspension by oral gavage according to the experimental schedule;

control animals received the same volume of anaerobic PBS. For comparisons involving wild-type P. distasonis, P. distasonis Δ5βR, and P. distasonis Δ5βR plus isoLCA, bacterial preparations were normalized to the same viable cell density before dosing. Comparable growth and viability of the parental and deletion strains were confirmed before animal administration.

2.8 Untargeted metabolomics and bile acid analysis

Serum from vehicle- and P. distasonis-treated mice was collected at the experimental endpoint, separated at 4°C, and stored at −80°C until analysis. Metabolites were extracted with prechilled methanol/acetonitrile/water (2:2:1, v/v/v), vortexed, sonicated on ice, and centrifuged at 12,000 × g for 15 min at 4°C. Supernatants were dried under vacuum and reconstituted in 50% methanol. A pooled quality-control sample generated by combining aliquots from study samples was injected at regular intervals to monitor analytical stability. Metabolites were analyzed by ultra-high-performance liquid chromatography coupled to tandem mass spectrometry in positive- and negative-ionization modes. Features were detected, aligned, deconvoluted, normalized, and annotated using authentic standards where available and spectral-library matching. Differential metabolites were defined using fold change, statistical significance, and multivariable importance criteria with false-discovery-rate correction. KEGG pathway enrichment was performed on annotated differential metabolites. Bile acid features were analyzed separately, and isoLCA assignment was confirmed by matching chromatographic retention and fragmentation behavior to the reference standard.

2.9 isoLCA administration

isoLCA was prepared in a vehicle compatible with oral exposure and supplied in drinking water at 20 μM for the indicated in vivo experiments. Solutions were protected from light and replaced regularly. Control mice received vehicle alone. Water intake and body weight were monitored to exclude treatment-related differences in fluid consumption. For rescue experiments, the same isoLCA regimen was administered to mice receiving the P. distasonis Δ5BR strain.

2.10 Shotgun metagenomics and bile acid enzyme screening

Microbial DNA from fecal samples was used to construct paired-end shotgun

metagenomic libraries. After sequencing, adapters, low-quality reads, and host-derived sequences were removed. High-quality reads were assembled, open reading frames were predicted, and genes were annotated against KEGG, eggNOG, and the NCBI non-redundant protein database. Taxonomic assignment and gene abundance were derived from the same filtered dataset. The functional screen focused on genes encoding 5β-reductase and 3β-hydroxysteroid dehydrogenase. Candidate sequences were retained when functional annotation and taxonomic placement were concordant. Taxa carrying either enzyme or both enzymes were summarized in a presence/absence matrix, and the isoLCA-related pathway was reconstructed from the annotated enzyme set.

2.11 Generation of the 5β-reductase-deficient P. distasonis strain

An isogenic 5β-reductase-deficient P. distasonis strain was generated by allelic exchange using homologous regions flanking the annotated 5β-reductase coding sequence. Recombinants were selected under anaerobic conditions and screened by junction PCR. Loss of the target open reading frame was confirmed by sequencing, while the corresponding wild-type locus was retained in the parental control strain. Wild-type and deletion strains were expanded in parallel, normalized by viable cell density, and tested for comparable growth before use in vivo.

2.12 RNA sequencing and pathway analysis

Total RNA was isolated from independent vehicle- and isoLCA-treated primary chondrocyte cultures using phenol–guanidinium extraction. RNA purity was assessed spectrophotometrically and integrity by capillary electrophoresis. Poly(A)-enriched libraries were constructed and sequenced as paired-end reads on an Illumina NovaSeq platform. Reads were filtered to remove adapters and low-quality bases, aligned to the mouse reference genome with a splice-aware aligner, and summarized at the gene level. Differential expression was analyzed using DESeq2. Genes with an adjusted P value < 0.05 and $|\log_2$ fold change$| > 1$ were considered differentially expressed. Gene set enrichment analysis was performed on the ranked gene list using curated pathway collections. Gene Ontology biological-process enrichment was performed on the differential gene set with multiple-testing correction.

2.13 Extracellular-flux analysis of mitochondrial respiration

Oxygen consumption was measured in live primary chondrocytes using a Seahorse extracellular-flux analyzer. Cells were plated at equal density in Seahorse cell-culture microplates and treated with vehicle or isoLCA. Before analysis, cultures were equilibrated in phenol-red- and bicarbonate-free assay medium adjusted to pH 7.4 in a non-CO_2 incubator. Basal oxygen-consumption rate (OCR) was recorded before sequential injection of oligomycin, FCCP, and rotenone/antimycin A. Basal respiration, ATP-linked respiration, maximal respiration, and spare respiratory capacity were calculated after subtraction of non-mitochondrial OCR and normalized to cell content. Three independent chondrocyte preparations were analyzed per condition.

2.14 Reactive oxygen species and mitochondrial membrane potential

Cellular ROS were measured using a cell-permeable oxidation-sensitive fluorescent probe. Vehicle- and isoLCA-treated cells were stained in parallel, washed, and analyzed using identical acquisition settings; fluorescence intensity was normalized to cell number or reported as mean fluorescence intensity according to the Figure 6 dataset. Mitochondrial membrane potential was assessed with JC-1. Red fluorescent aggregates and green monomers were quantified by flow cytometry, and the aggregate-to-monomer fluorescence ratio was used as the membrane-potential index. Unstained and single-color controls were included for gating and compensation.

2.15 Senescence-associated β-galactosidase staining

Primary chondrocytes were fixed briefly and incubated with senescence-associated β-galactosidase staining solution at pH 6.0 overnight at 37°C in a non-CO_2 environment. Cells were imaged by bright-field microscopy under identical acquisition conditions. The proportion of blue-stained cells was quantified from randomly selected fields by an investigator blinded to treatment group.

2.16 Immunofluorescence

Paraffin-embedded joint sections were deparaffinized, rehydrated, subjected to antigen retrieval, and blocked to reduce nonspecific binding. Sections were incubated with primary antibodies against p16 or p21, followed by species-appropriate fluorescent secondary antibodies and DAPI nuclear counterstaining. Images were acquired under identical exposure settings. Positive cells were quantified in predefined articular-cartilage

regions by a blinded investigator. For all quantitative imaging analyses, the same thresholding and region-of-interest rules were applied across groups within an experiment.

2.17 Micro-computed tomography

Knee joints were fixed in 4% paraformaldehyde for 24–48 h at 4°C and scanned before decalcification. Scanning was performed at approximately 50 kV and 200 μA with an isotropic voxel size of approximately 10 μm. Three-dimensional reconstruction and quantitative analysis were performed using identical thresholds for all samples within an experiment. Osteophyte number and total osteophyte volume were measured within a standardized periarticular region of interest. Calcified-cartilage thickness and related structural parameters were measured on aligned sections using consistent anatomic landmarks. Analysts were blinded to treatment group.

2.18 Histology and OARSI scoring

Following micro-CT, knee joints were decalcified in 10% EDTA at 4°C for 3–4 weeks with regular solution replacement, dehydrated, paraffin embedded, and sectioned sagittally at 5 μm. Safranin O/Fast Green staining was used to evaluate articular-cartilage architecture and proteoglycan loss, and hematoxylin/eosin staining was used to assess synovial morphology. Cartilage degeneration was graded using the murine OARSI histopathology system [20]. Synovitis was graded according to lining thickness, stromal cellularity, and inflammatory-cell infiltration. Sections were scored by blinded observers, and quantitative image measurements were obtained from anatomically matched regions using identical analysis settings.

2.19 Quantification and statistical analysis

Data are presented as mean ± SD with individual biological replicates shown in quantitative plots. For two-group comparisons, two-sided unpaired Student's t tests were used when parametric assumptions were satisfied; nonparametric alternatives were used when appropriate. Experiments containing more than two treatment groups were analyzed by one-way ANOVA with multiplicity-adjusted post hoc testing. A two-sided $P < 0.05$ was considered statistically significant. For experiments involving two independent variables (genotype × treatment), two-way ANOVA followed by multiplicity-adjusted post hoc comparisons was used. *$P < 0.05$, **$P < 0.01$, and ***$P < 0.001$; "ns" means no statistically

significant difference.

3 Results

3.1 Exercise suppresses joint degeneration and systemic inflammatory activity in experimental OA

Exercise is clinically beneficial in OA, but the extent to which this benefit is reflected in structural joint preservation remains incompletely explained. We therefore first established the phenotype produced by treadmill exercise in mice subjected to destabilization of the medial meniscus (DMM). Three-dimensional micro-computed tomography (micro-CT), Safranin O/Fast Green staining, and synovial histology consistently showed less severe joint damage in exercised mice than in sedentary DMM controls (Figure 1A–C). Exercise preserved cartilage proteoglycan content and surface architecture, reduced synovial thickening, and markedly limited periarticular osteophyte formation.

Quantitative analyses mirrored the representative pathology. Exercised mice showed lower OARSI scores and synovitis grades, reduced calcified cartilage thickness, fewer osteophytes, and a lower total osteophyte volume (Figure 1E). The mean OARSI score decreased from approximately 3.0 in control DMM mice to approximately 0.6 after exercise, while synovitis decreased from approximately 1.7 to 0.5. These structural effects were accompanied by a pronounced reduction in circulating inflammatory and matrix-remodeling mediators. Serum IL-1β, IL-6, and MMP-3 levels were also significantly lower in the exercise group than in the control group (Figure 1D).

Together, these data establish a robust disease-modifying phenotype in which exercise affects not only OA-associated inflammation but also cartilage integrity, synovial pathology, and osteophyte burden. This provided the experimental basis to ask whether a systemic, transferable signal contributes to the protection generated by exercise.

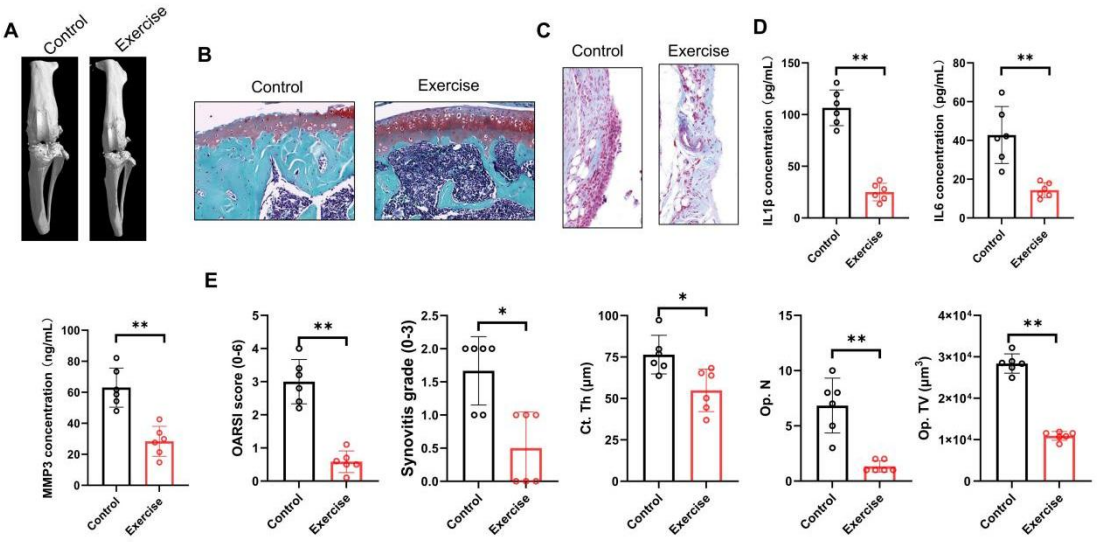


Figure 1. Exercise attenuates experimental osteoarthritis and systemic inflammation. (A) Representative three-dimensional micro-CT reconstructions of knee joints from control and exercised DMM mice. (B) Representative Safranin O/Fast Green-stained sections showing articular-cartilage preservation after exercise. (C) Representative synovial histology. (D) Serum concentrations of IL-1β, IL-6, and MMP-3. (E) Quantification of OARSI score, synovitis grade, calcified-cartilage thickness (Ct.Th), osteophyte number (Op.N), and total osteophyte volume (Op.TV). n = 6 mice per group. Data are mean ± SD. Two-sided unpaired tests were used for two-group comparisons; *P < 0.05, **P < 0.01.

3.2 Exercise-conditioned intestinal bacteria and metabolites are sufficient to transfer OA protection

Because exercise altered both joint structure and systemic inflammatory mediators, we next asked whether the intestinal ecosystem could carry part of this protective information independently of the recipient animal performing exercise. Fresh feces from exercised donor mice were separated into whole fecal material, a microbial cellular fraction, and a sterile cell-free metabolite fraction. Each preparation was administered orally to recipient mice before DMM induction and during the experimental period, followed by blinded structural and inflammatory assessment (Figure 2A).

Remarkably, all three exercise-derived preparations improved joint pathology relative to control-treated recipients. Safranin O/Fast Green staining demonstrated preservation of

cartilage matrix, micro-CT showed reduced osteophyte formation, and synovial histology showed attenuated inflammatory remodeling (Figure 2B–D). The mean OARSI score was higher in control recipients but significance decreased in mice receiving whole fecal material, the bacterial fraction, and the metabolite fraction, respectively. Synovitis followed the same pattern. Calcified cartilage thickness, osteophyte number, and osteophyte volume were also reduced across all exercise-derived preparations (Figure 2F).

The transferred structural benefit was accompanied by lower circulating IL-1β, IL-6, and MMP-3 (Figure 2E). The activity retained by the microbial fraction indicates that the cellular microbial component is sufficient to transmit protection, whereas the comparable activity of the sterile fraction demonstrates that diffusible products can reproduce a substantial component of the phenotype without transfer of intact donor bacteria. Thus, the intestinal response to exercise contains both a microbial source and a soluble downstream effector.

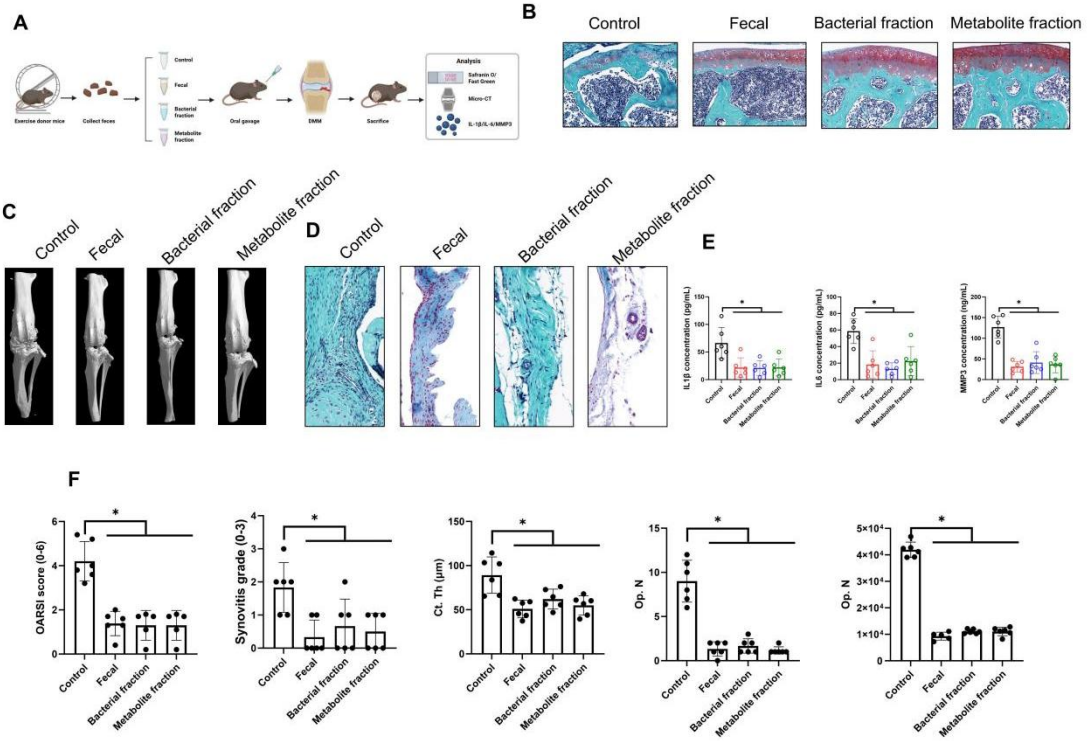


Figure 2. Exercise-derived fecal bacteria and cell-free metabolites transfer protection against OA.

(A) Experimental workflow showing fecal collection from exercised donors, separation into whole fecal material, microbial cellular fraction, and sterile metabolite fraction, oral transfer

to recipients, DMM surgery, and endpoint analysis. (B) Representative Safranin O/Fast Green staining. (C) Representative three-dimensional micro-CT reconstructions. (D) Representative synovial histology. (E) Serum IL-1β, IL-6, and MMP-3. (F) OARSI score, synovitis grade, calcified-cartilage thickness, osteophyte number, and osteophyte volume. n = 6 mice per group. Data are mean ± SD. One-way ANOVA with multiplicity-adjusted post hoc comparisons was used; *P < 0.05.

3.3 Exercise selectively enriches P. distasonis, which restrains cartilage degeneration and chondrocyte senescence

To resolve the microbial component of the transferable phenotype, we profiled fecal communities from control and exercised mice by 16S rRNA gene sequencing (Figure 3A). Bray–Curtis principal coordinate analysis separated the two groups, and PERMANOVA confirmed a significant difference in overall community structure (Figure 3B). Genus-level composition, hierarchical clustering, and LEfSe analyses revealed coordinated remodeling across multiple taxa (Figure 3C–E). Among the exercise-associated organisms, P. distasonis showed one of the most pronounced and consistent enrichments(Figure 3F).

We therefore tested whether P. distasonis was sufficient to reproduce the exercise-associated joint phenotype. Mice receiving live P. distasonis by oral gavage developed substantially less severe OA than vehicle-treated controls. Micro-CT and Safranin O/Fast Green staining showed reduced osteophyte formation and preservation of cartilage architecture (Figure 3G–I). Quantitatively, OARSI scores, calcified cartilage thickness, osteophyte number and osteophyte volume were all significantly reduced compared with the PBS-treated group (Figure 3H).

Because mitochondrial dysfunction and cellular senescence are tightly linked to OA progression, we next examined whether bacterial treatment altered the senescence state of cartilage. P. distasonis markedly reduced p16- and p21-positive chondrocytes in articular cartilage (Figure 3J, K) and decreased senescence-associated β-galactosidase staining in primary chondrocytes (Figure 3L). Thus, an organism strongly enriched by exercise is sufficient to reproduce both structural joint protection and an antisenescence phenotype, positioning P. distasonis as a candidate upstream mediator of the exercise-conditioned

intestinal signal.

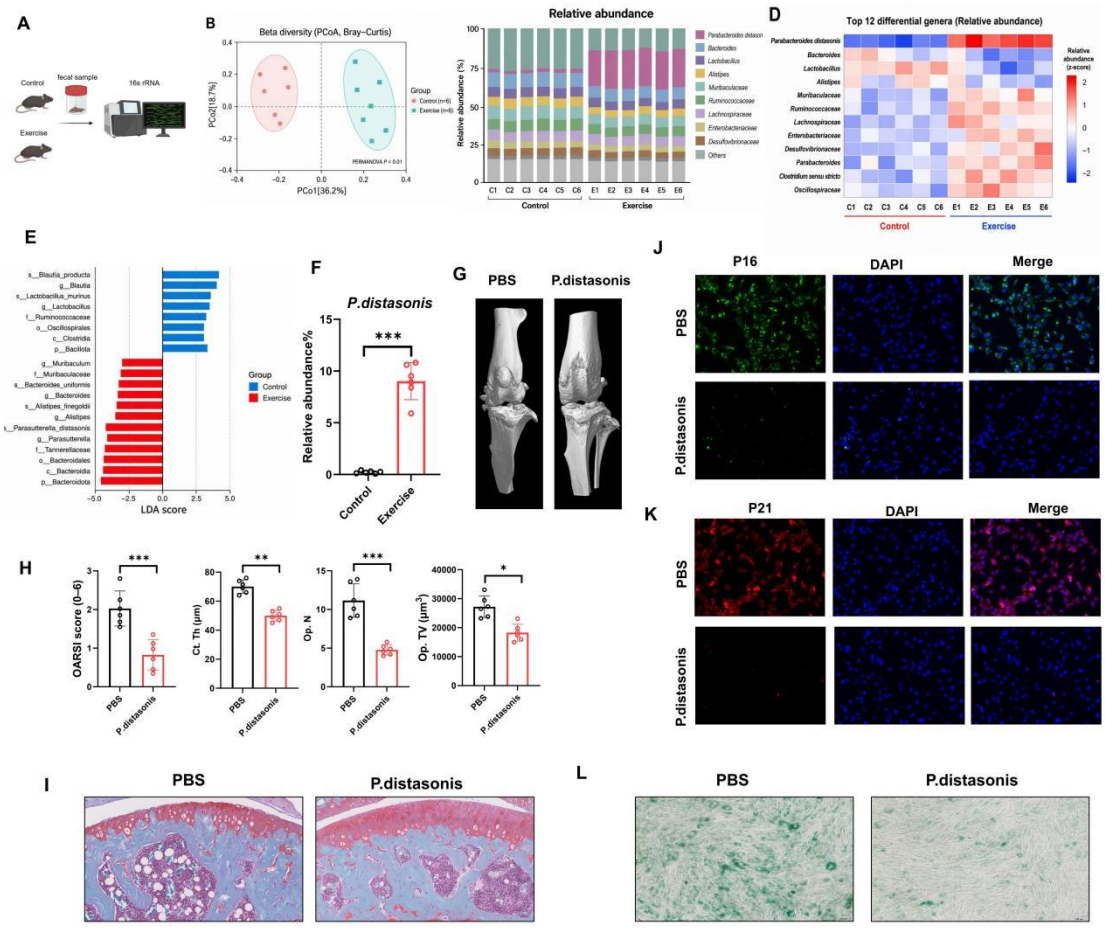


Figure 3. Exercise enriches P. distasonis, which protects the joint and suppresses chondrocyte senescence.

Workflow for fecal 16S rRNA gene sequencing of control and exercised mice. (B) Bray–Curtis principal coordinate analysis showing separation of control and exercise-associated microbial communities; group difference assessed by PERMANOVA. (C) Genus-level relative-abundance profiles. (D) Heatmap of the top differential taxa. (E) LEfSe analysis of discriminating taxa. (F) Relative abundance of P. distasonis. (G) Representative micro-CT reconstructions after vehicle or P. distasonis gavage. (H) Quantification of OARSI score, calcified-cartilage thickness, osteophyte number, and osteophyte volume. (I) Representative Safranin O/Fast Green staining. (J, K) Representative p16 and p21 immunofluorescence in articular cartilage. (L) Senescence-associated β-galactosidase staining of primary chondrocytes. n = 6 mice per group for in vivo experiments. Data are mean ± SD. *P < 0.05, **P < 0.01, ***P < 0.001.

3.4 P. distasonis remodels bile acid metabolism and identifies isoLCA as a cartilage-protective metabolite

The finding that a sterile exercise-derived metabolite fraction retained activity suggested that a diffusible microbial product might mediate the effect of P. distasonis. We therefore performed untargeted metabolomic profiling after P. distasonis administration. Pathway enrichment analysis identified bile secretion, primary bile acid biosynthesis, and secondary bile acid biosynthesis among the most prominently altered metabolic programs (Figure 4A). The global volcano plot showed broad metabolite remodeling, and isoLCA emerged among the most strongly increased features (Figure 4B). A bile acid-focused heatmap further demonstrated a distinct metabolic signature in P. distasonis-treated mice, with isoLCA showing a particularly pronounced increase (Figure 4C). Direct quantification confirmed an increase from 0.07 ± 0.02 to 10.23 ± 3.76 in the normalized LC–MS readout (Figure 4D).

To determine whether isoLCA was functionally sufficient, we administered isoLCA directly to mice with DMM-induced OA. isoLCA improved micro-CT and histological features of disease (Figure 4E, F). OARSI score,calcified cartilage thickness, osteophyte number and osteophyte volume werer significantly decreased (Figure 4G). Consistent with the phenotype produced by P. distasonis, isoLCA also reduced senescence-associated β-galactosidase postive cells and decreased p16 and p21 staining (Figure 4H–J).

These data identify isoLCA as a bioactive metabolite capable of reproducing major structural and antisenescence effects of P. distasonis. The convergence of the fecal-fractionation experiment and the targeted bacterial metabolomics therefore suggested a mechanistic sequence in which exercise alters the intestinal microbial community, P. distasonis expands, and a bile acid-derived soluble product communicates with the joint.

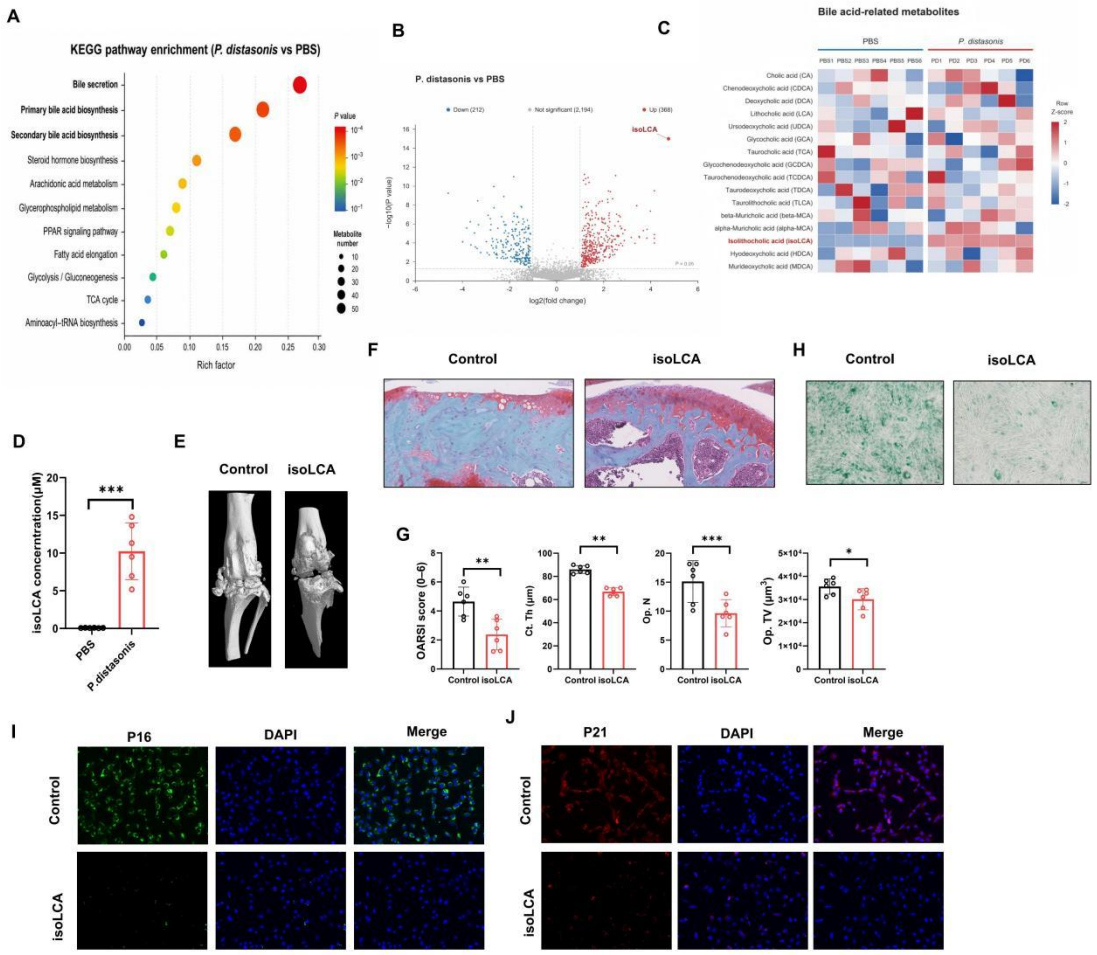


Figure 4. P. distasonis remodels bile acid metabolism and isoLCA reproduces joint protection.

(A) KEGG pathway enrichment of metabolites altered by P. distasonis treatment. (B) Volcano plot of differential metabolites, with isoLCA highlighted. (C) Heatmap of bile acid-related metabolites in vehicle- and P. distasonis-treated mice. (D) Quantification of isoLCA. (E) Representative micro-CT reconstructions of control and isoLCA-treated DMM joints. (F) Representative Safranin O/Fast Green staining. (G) Quantification of OARSI score, calcified-cartilage thickness, osteophyte number, and osteophyte volume. (H) Senescence-associated β-galactosidase staining. (I,J) Representative p16 and p21 immunofluorescence. n = 6 mice per group for in vivo experiments. Data are mean ± SD. *P < 0.05, **P < 0.01, ***P < 0.001.

3.5 Bacterial 5β-reductase is required for the P. distasonis–isoLCA protective pathway

Direct isoLCA administration established metabolite sufficiency but did not demonstrate that the protective activity of P. distasonis depends on isoLCA production. We therefore interrogated shotgun metagenomic data for enzymes positioned along the isoLCA biosynthetic route (Figure 5A). isoLCA production relies on 5BR and 3β-hydroxysteroid dehydrogenase (Figure 5B). Among the detected taxa, only Clostridium innocuum, P. distasonis, and one Lachnospiraceae taxon encoded both enzymatic activities (Figure 5C). P. distasonis was therefore distinguished by combining strong exercise responsiveness with the relevant isoLCA metabolic capacity.

We next generated an isogenic P. distasonis strain lacking 5β-reductase (P. distasonis Δ5BR) and compared its activity with wild-type bacteria. Wild-type P. distasonis markedly protected the DMM joint, whereas deletion of 5β-reductase abolished the protective phenotype. Importantly, exogenous isoLCA restored protection in mice receiving the Δ5BR strain (Figure 5D, E). OARSI score,calcified cartilage thickness, osteophyte number and osteophyte volume werer significantly decreased in Wild-type P. distasonis treated group,but not in P.distasonis△5BR Group (Figure 5F). Overall, 5β-reductase activity and isoLCA production are required for P. distasonis-mediated joint protection.

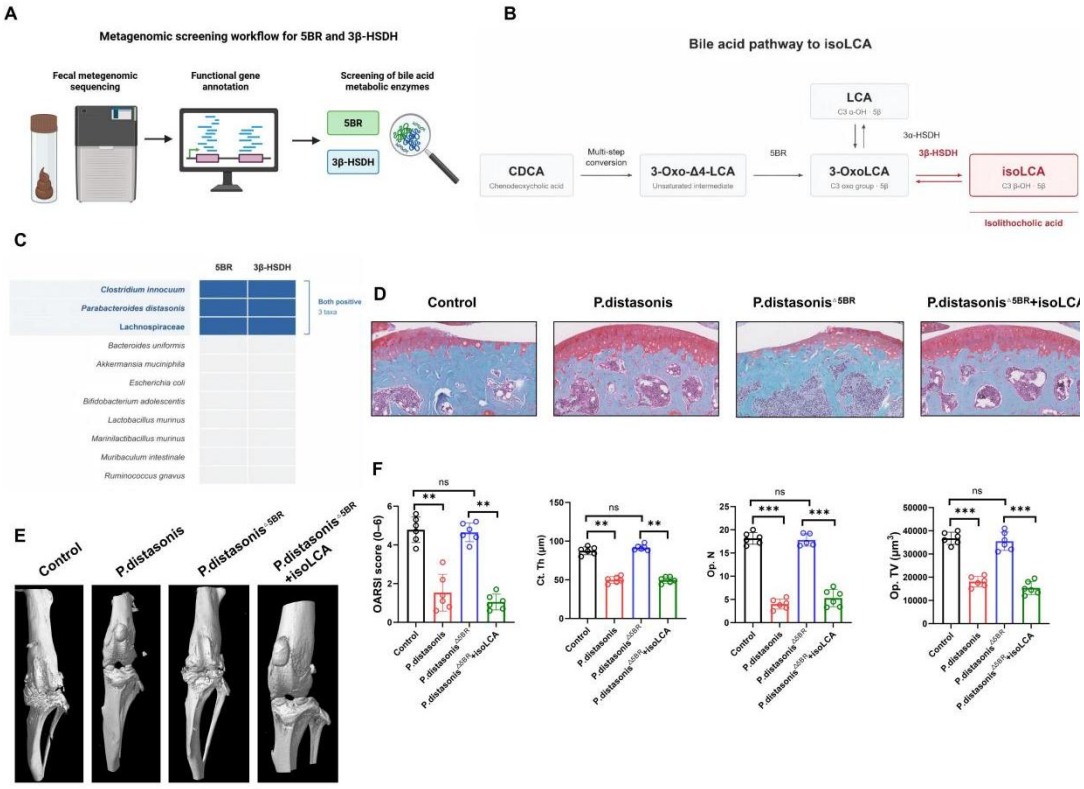


Figure 5. Bacterial 5β-reductase is required for P. distasonis-mediated OA protection. (A) Metagenomic workflow used to screen microbial taxa for 5β-reductase (5BR) and 3β-hydroxysteroid dehydrogenase (3β-HSDH). (B) Reconstructed bile acid pathway leading to isoLCA. (C) Presence/absence matrix of 5BR and 3β-HSDH across detected taxa; three taxa encoded both activities. (D) Representative Safranin O/Fast Green staining of joints from control mice and mice receiving wild-type P. distasonis, P. distasonis Δ5BR, or P. distasonis Δ5BR plus isoLCA. (E) Representative micro-CT reconstructions. (F) Quantification of OARSI score, calcified-cartilage thickness, osteophyte number, and osteophyte volume. n = 6 mice per group. Data are mean ± SD. One-way ANOVA with multiplicity-adjusted post hoc comparisons was used; ns, not significant; **P < 0.01, ***P < 0.001.

3.6 isoLCA activates a PGC-1α-centered mitochondrial program in chondrocytes

We next asked how isoLCA acts within cartilage. Primary chondrocytes were treated with isoLCA or vehicle and subjected to RNA sequencing. isoLCA induced broad transcriptional remodeling, with 1,316 genes upregulated and 1,148 genes downregulated at the prespecified differential-expression threshold (Figure 6A).

Consistent with this observation, gene set enrichment analysis demonstrated a pronounced enrichment of the oxidative phosphorylation program in isoLCA-treated chondrocytes (NES = 2.32, FDR q < 0.001; Figure 6B). Functional enrichment analysis further revealed coordinated activation of mitochondrial processes, including mitochondrial organization, electron transport, ATP metabolism, respiratory-chain complex assembly, fatty-acid β-oxidation, mitochondrial translation, the tricarboxylic acid cycle, and mitochondrial membrane organization (Figure 6C). These transcriptional changes suggested that isoLCA does not simply suppress catabolic responses, but instead induces a broad mitochondrial remodeling program in chondrocytes.

We next validated the induction of PGC-1α independently. Quantitative analysis confirmed a marked increase in Ppargc1a expression after isoLCA treatment, reaching approximately sixfold that observed in vehicle-treated cells (Figure 6D). We therefore asked whether this transcriptional response translated into restoration of mitochondrial

integrity. Flow-cytometric analysis of intracellular reactive oxygen species showed that isoLCA substantially reduced oxidative stress, as reflected by a decrease in fluorescence intensity compared with control chondrocytes (Figures 6E, 6F). In parallel, JC-1 analysis revealed a pronounced shift toward mitochondrial aggregates and a corresponding increase in the aggregate-to-monomer fluorescence ratio, indicating restoration of mitochondrial membrane potential (Figure 6G).

To directly determine whether these changes were accompanied by improved mitochondrial bioenergetics, we measured oxygen consumption using Seahorse extracellular flux analysis. isoLCA markedly increased oxygen consumption throughout the mitochondrial stress test and substantially enhanced basal respiration, maximal respiration, ATP-linked respiration, and spare respiratory capacity compared with vehicle-treated cells (Figure 6H).

Together, these findings identify PGC-1α-associated mitochondrial reprogramming as a major cellular response to isoLCA, linking the microbial bile acid signal to restoration of chondrocyte redox homeostasis, membrane polarization, and oxidative metabolism. These observations prompted us to next determine whether PGC-1α is merely associated with this response or is functionally required for the cartilage-protective effect of isoLCA in vivo.

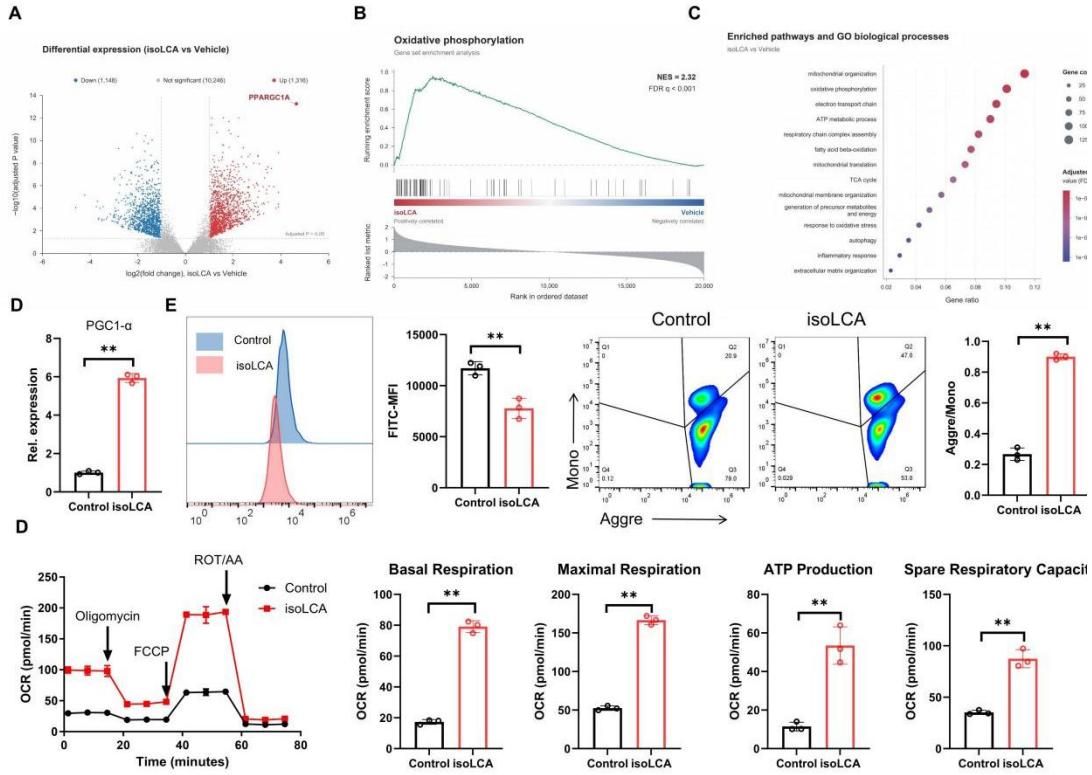


Figure 6. isoLCA activates PGC-1α and restores mitochondrial function in chondrocytes

(A) Volcano plot showing differentially expressed genes in primary chondrocytes treated with isoLCA versus vehicle. (B) Gene set enrichment analysis showing significant enrichment of the oxidative phosphorylation pathway in isoLCA-treated chondrocytes (NES = 2.32, FDR q < 0.001). (C) Bubble plot showing enriched pathways and Gene Ontology biological processes after isoLCA treatment. (D) Relative expression of Ppargc1a (PGC-1α) in primary chondrocytes treated with vehicle or isoLCA. (E) Representative flow-cytometric histograms of intracellular reactive oxygen species in vehicle- and isoLCA-treated chondrocytes. (F) Quantification of intracellular ROS fluorescence intensity expressed as FITC mean fluorescence intensity. (G) Representative JC-1 flow-cytometry plots and quantification of the mitochondrial JC-1 aggregate-to-monomer fluorescence ratio in vehicle- and isoLCA-treated chondrocytes. (H) Seahorse XF mitochondrial stress-test analysis of vehicle- and isoLCA-treated primary chondrocytes. Data are presented as mean ± SD. Statistical significance was determined using a two-tailed unpaired Student's t test. **P < 0.01.

3.7 Cartilage PGC-1α is required for isoLCA-mediated protection in vivo

The induction of PGC-1α in cultured chondrocytes suggested a candidate host effector, but it remained essential to determine whether this pathway was required for disease modification in vivo. We therefore compared tamoxifen-inducible cartilage-lineage PGC-1α-deficient mice (Col2a1-CreERT2; Ppargc1a^fl/fl) with Ppargc1a^fl/fl littermate controls in the DMM model, with or without isoLCA administration (Figure 7A).

isoLCA strongly improved cartilage histology and joint architecture in Ppargc1a^fl/fl controls but failed to provide comparable protection after cartilage-lineage PGC-1α deletion (Figure 7B, C). In floxed controls, the OARSI score decreased with isoLCA treatment. In conditional knockout mice, no significant reduction was observed. Calcified cartilage thickness, osteophyte number, and osteophyte volume showed the same genotype-by-treatment pattern: isoLCA improved each outcome in Ppargc1a^fl/fl mice, whereas the response was lost or markedly attenuated in Col2a1-CreERT2; Ppargc1a^fl/fl mice (Figure 7D).

The inflammatory readouts followed the structural phenotype. isoLCA reduced circulating IL-1β, IL-6, and MMP-3 in floxed controls, but these reductions were absent or strongly blunted after PGC-1α deletion (Figure 7E). These genetic data establish cartilage PGC-1α as a necessary host effector for the joint-protective action of isoLCA and complete a causal pathway from exercise-induced microbial remodeling to chondrocyte mitochondrial homeostasis.

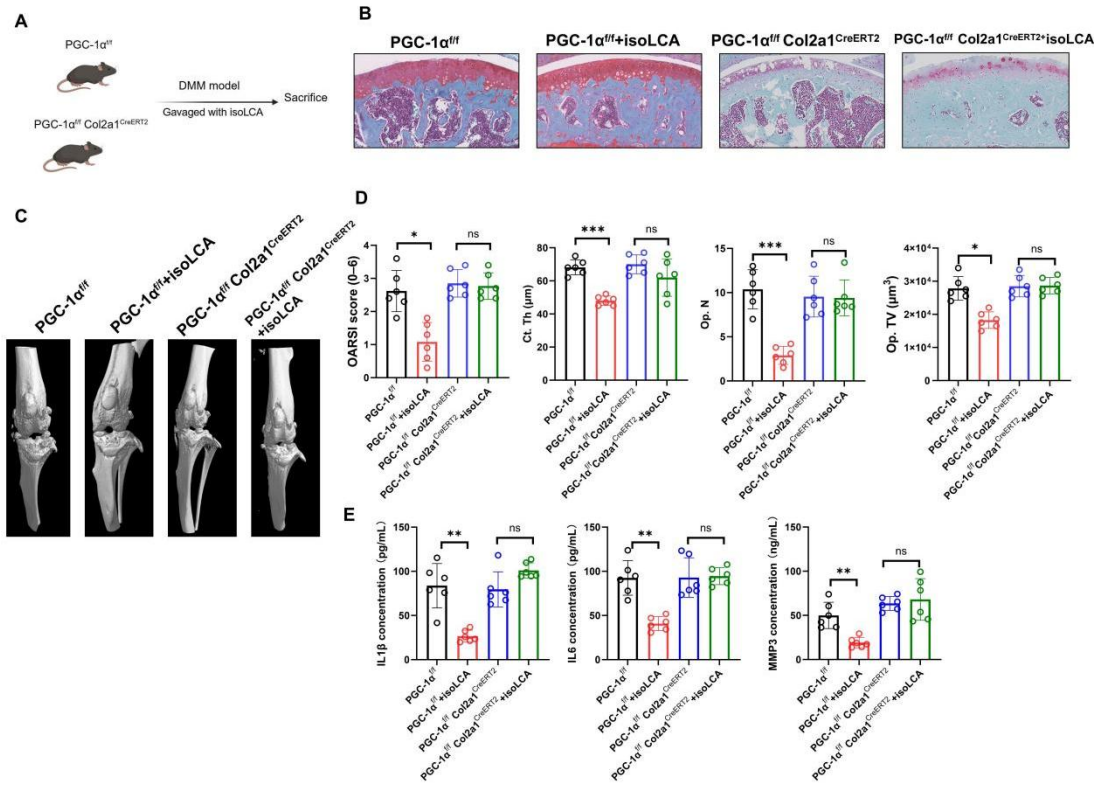


Figure 7. Cartilage-lineage PGC-1α is required for isoLCA-mediated protection.

(A) Experimental design using Ppargc1a^fl/fl littermate controls and Col2a1-CreERT2; Ppargc1a^fl/fl mice subjected to DMM with or without isoLCA. (B) Representative Safranin O/Fast Green staining. (C) Representative three-dimensional micro-CT reconstructions. (D) Quantification of OARSI score, calcified-cartilage thickness, osteophyte number, and osteophyte volume. (E) Serum IL-1β, IL-6, and MMP-3. n = 6 mice per group. Data are mean ± SD. Two-way ANOVA with multiplicity-adjusted post hoc comparisons was used; ns, not significant; *P < 0.05, **P < 0.01, ***P < 0.001.

4 Discussion

Exercise is a cornerstone of OA management, yet the biological logic connecting physical activity to cartilage preservation has remained fragmented. The present study identifies a defined intestinal pathway that carries a substantial component of this effect. The data support a sequential model in which exercise remodels the gut microbiota, markedly enriches P. distasonis, and increases a bacterial bile acid program that generates isoLCA. isoLCA then acts on chondrocytes to induce PGC-1α, restore oxidative

metabolism, reduce mitochondrial stress, and suppress senescence. Importantly, each major transition in this pathway is supported by a functional experiment: exercise-derived fecal material transfers protection; P. distasonis is sufficient to reproduce it; bacterial 5β-reductase deletion removes protection; exogenous isoLCA rescues the bacterial defect; and cartilage-lineage PGC-1α deletion prevents isoLCA from protecting the joint. This layered loss-and-rescue strategy distinguishes the pathway from a simple correlation between exercise, microbial composition, and OA severity.

The fecal fractionation experiment is particularly important because it moves the mechanism beyond local biomechanics. Exercise undoubtedly changes muscle strength, gait, joint loading, neuroendocrine signaling, and systemic metabolism. None of those mechanisms is excluded by our data. However, the ability of material collected from exercised donors to protect non-exercising recipients demonstrates that an intestinal signal is independently sufficient to modify structural OA. Protection by the microbial fraction indicates that the exercise-conditioned microbial community can carry this signal, whereas activity in the sterile fraction demonstrates that intact donor organisms are not required once the relevant soluble products are present. This division of activity provides a conceptual bridge between a live-biotherapeutic mechanism and a postbiotic mechanism.

P. distasonis emerged as the species-level connection between exercise and the metabolite response. Exercise increased its relative abundance from a nearly undetectable baseline to approximately 9% of the measured community, and direct gavage was sufficient to reduce cartilage damage, osteophyte burden, and chondrocyte senescence. P. distasonis has previously been implicated in regulation of bile acid metabolism, metabolic homeostasis, and inflammatory arthritis [12-14]. Our findings extend these observations in three ways. First, they place P. distasonis downstream of a physiological intervention rather than exogenous probiotic administration alone. Second, they connect its activity to injury-induced OA rather than only systemic inflammatory disease. Third, the bacterial deletion and metabolite-rescue experiments identify a specific enzymatic pathway rather than attributing protection to nonspecific colonization or global microbial competition.

The 5β-reductase loss-and-rescue experiment provides the most direct evidence for the order of the microbial pathway. Wild-type P. distasonis was protective, the isogenic

Δ5βR strain was not, and isoLCA bypassed the genetic defect. This pattern is difficult to explain by differences in bacterial exposure alone and places 5β-reductase upstream of the metabolite-mediated effect. Metagenomic screening further showed that the combined 5β-reductase and 3β-hydroxysteroid dehydrogenase capacity was restricted to a small subset of detected taxa, while P. distasonis uniquely combined this enzymatic repertoire with strong exercise responsiveness. The data therefore nominate a microbial metabolic function, rather than taxonomic abundance per se, as the key unit of causality.

isoLCA has been studied primarily as an immunomodulatory bile acid that can restrain Th17 differentiation and influence peripheral immune homeostasis [9-11]. Our data reveal a distinct cartilage-intrinsic dimension of isoLCA biology. In primary chondrocytes, the dominant transcriptional response was not limited to inflammatory suppression but instead centered on oxidative phosphorylation, mitochondrial organization, electron transport, fatty acid oxidation, and ATP metabolism. This response was accompanied by a several-fold induction of Ppargc1a, increased basal and maximal respiration, increased ATP-linked respiration and spare respiratory capacity, reduced ROS, and recovery of mitochondrial membrane potential. These changes are mechanistically coherent with the established role of mitochondrial dysfunction in OA, in which reduced respiratory efficiency and excess oxidative stress promote matrix catabolism and cellular senescence [15-19].

The conditional knockout experiment further narrows the mechanism. isoLCA improved both structural and inflammatory readouts in Ppargc1a^fl/fl controls but lost efficacy when PGC-1α was deleted in the cartilage lineage. Thus, a systemic metabolite requires an intact chondrocyte metabolic program to modify disease. This does not exclude additional actions of isoLCA on intestinal, immune, synovial, bone, or vascular cells; indeed, bile acids are pleiotropic signaling molecules. Rather, the genetic data establish that cartilage PGC-1α is not merely a biomarker induced in parallel with protection but an essential host effector in the observed pathway. The result also provides a conceptual explanation for how an intestinal metabolite can influence an avascular tissue: the critical signal need not be sustained immune-cell infiltration if it can reprogram the metabolic state of resident chondrocytes.

This work also reframes the systemic biology of exercise in OA. Exercise-induced

microbiome changes have been documented across human and animal studies, including alterations in community structure, functional pathways, and microbial metabolite output [3-6]. Most work in this field has focused on exercise performance or cardiometabolic health. Our findings indicate that an exercise-responsive microbial program can influence a degenerative musculoskeletal disease and identify a defined bacterium–enzyme–metabolite–host-effector chain. This may help explain why the benefits of exercise in OA extend beyond changes in body weight or local joint mechanics, while remaining fully compatible with those established mechanisms.

The pathway has potential translational implications but should not be interpreted as a substitute for exercise. Physical activity produces broad musculoskeletal, cardiovascular, metabolic, and neurobehavioral benefits that cannot be reduced to a single microbial metabolite. Instead, P. distasonis or isoLCA-like postbiotics could represent complementary strategies for individuals whose pain, frailty, comorbidity, or advanced disability limits exercise exposure. The bacterial genetic data further suggest that microbial enzyme capacity could be used to stratify or engineer candidate live biotherapeutics. Such approaches will require rigorous pharmacokinetic, toxicological, colonization, and dose-response studies because bile acids have concentration-, tissue-, and receptor-dependent effects.

In summary, our study defines a gut microbial mechanism by which exercise can be translated into cartilage protection. Exercise enriches P. distasonis, bacterial 5β-reductase enables an isoLCA-producing pathway, and isoLCA restores chondrocyte mitochondrial fitness through PGC-1α. The convergence of microbial transfer, bacterial genetics, metabolite rescue, transcriptional profiling, bioenergetic analysis, and cartilage-specific host genetics establishes a causal exercise–microbiota–metabolite–mitochondria axis in OA.

Declarations

Ethics approval and consent to participate

All animal experiments were approved by the Experimental Animal Ethics Committee of Yangzhou University (Approval No. yzu-lcyxy-n008) and were conducted in accordance

with national guidelines for laboratory animal welfare. Consent to participate was not applicable because this study did not involve human participants.

Consent for publication

Not applicable.

Competing interests

The authors declare that they have no competing interests.

Funding

This research was supported by the Jiangsu Province's Double Innovation Plan (Grant No. JSSCBS20230496).

Acknowledgements

Not applicable.

Authors' information

Not applicable.

References

1. Kolasinski SL, Neogi T, Hochberg MC, et al. 2019 American College of Rheumatology/Arthritis Foundation guideline for the management of osteoarthritis of the hand, hip, and knee. Arthritis Rheumatol. 2020;72:220–233. doi:10.1002/art.41142.

2. Bannuru RR, Osani MC, Vaysbrot EE, et al. OARSI guidelines for the non-surgical management of knee, hip, and polyarticular osteoarthritis. Osteoarthritis Cartilage. 2019;27:1578–1589. doi:10.1016/j.joca.2019.06.011.

3. Allen JM, Mailing LJ, Niemiro GM, et al. Exercise alters gut microbiota composition and function in lean and obese humans. Med Sci Sports Exerc. 2018;50:747–757. doi:10.1249/MSS.0000000000001495.

4. Barton W, Penney NC, Cronin O, et al. The microbiome of professional athletes differs

from that of more sedentary subjects in composition and particularly at the functional metabolic level. Gut. 2018;67:625–633. doi:10.1136/gutjnl-2016-313627.

5. Scheiman J, Luber JM, Chavkin TA, et al. Meta-omics analysis of elite athletes identifies a performance-enhancing microbe that functions via lactate metabolism. Nat Med. 2019;25:1104–1109. doi:10.1038/s41591-019-0485-4.

6. Min L, Ablitip A, Wang R, et al. Effects of exercise on gut microbiota of adults: a systematic review and meta-analysis. Nutrients. 2024;16:1070. doi:10.3390/nu16071070.

7. Ulici V, Kelley KL, Azcarate-Peril MA, et al. Osteoarthritis induced by destabilization of the medial meniscus is reduced in germ-free mice. Osteoarthritis Cartilage. 2018;26:1098–1109. doi:10.1016/j.joca.2018.05.016.

8. Schott EM, Farnsworth CW, Grier A, et al. Targeting the gut microbiome to treat the osteoarthritis of obesity. JCI Insight. 2018;3:e95997. doi:10.1172/jci.insight.95997.

9. Hang S, Paik D, Yao L, et al. Bile acid metabolites control TH17 and Treg cell differentiation. Nature. 2019;576:143–148. doi:10.1038/s41586-019-1785-z.

10. Campbell C, McKenney PT, Konstantinovsky D, et al. Bacterial metabolism of bile acids promotes generation of peripheral regulatory T cells. Nature. 2020;581:475–479. doi:10.1038/s41586-020-2193-0.

11. Paik D, Yao L, Zhang Y, et al. Human gut bacteria produce TH17-modulating bile acid metabolites. Nature. 2022;603:907–912. doi:10.1038/s41586-022-04480-z.

12. Sun H, Guo Y, Wang H, et al. Gut commensal Parabacteroides distasonis alleviates inflammatory arthritis. Gut. 2023;72:1664–1677. doi:10.1136/gutjnl-2022-327756.

13. Zhao Q, Dai MY, Huang RY, et al. Parabacteroides distasonis ameliorates hepatic fibrosis potentially via modulating intestinal bile acid metabolism and hepatocyte pyroptosis in male mice. Nat Commun. 2023;14:1829. doi:10.1038/s41467-023-37572-x.

14. Wang K, Liao M, Zhou N, et al. Parabacteroides distasonis alleviates obesity and metabolic dysfunctions via production of succinate and secondary bile acids. Cell Rep. 2019;26:222–235.e5. doi:10.1016/j.celrep.2018.12.028.

15. Coryell PR, Diekman BO, Loeser RF. Mechanisms and therapeutic implications of cellular senescence in osteoarthritis. Nat Rev Rheumatol. 2021;17:47–57. doi:10.1038/s41584-020-00533-7.

16. Jeon OH, Kim C, Laberge RM, et al. Local clearance of senescent cells attenuates the development of post-traumatic osteoarthritis and creates a pro-regenerative environment. Nat Med. 2017;23:775–781. doi:10.1038/nm.4324.

17. Mobasheri A, Rayman MP, Gualillo O, Sellam J, van der Kraan P, Fearon U. The role of metabolism in the pathogenesis of osteoarthritis. Nat Rev Rheumatol. 2017;13:302–311. doi:10.1038/nrrheum.2017.50.

18. Wang Y, Zhao X, Lotz M, Terkeltaub R, Liu-Bryan R. Mitochondrial biogenesis is impaired in osteoarthritis chondrocytes but reversible via peroxisome proliferator-activated receptor γ coactivator 1α. Arthritis Rheumatol. 2015;67:2141–2153. doi:10.1002/art.39182.

19. Wang H, Su J, Yu M, Xia Y, Wei Y. PGC-1α in osteoarthritic chondrocytes from mechanism to target of action. Front Pharmacol. 2023;14:1169019. doi:10.3389/fphar.2023.1169019.

20. Glasson SS, Chambers MG, Van Den Berg WB, Little CB. The OARSI histopathology initiative recommendations for histological assessments of osteoarthritis in the mouse. Osteoarthritis Cartilage. 2010;18(Suppl 3):S17–S23. doi:10.1016/j.joca.2010.05.025.